STUDY OF PASSIVE FILMS FORMED ON AISI 316L STAINLESS STEEL IN NON-POLLUTED AND POLLUTED SEAWATER FROM THE VOLCANO OF EL HIERRO ISLAND (SPAIN).

Fernández-Domene, R.M, Sánchez-Tovar, R., Escrivà-Cerdán, C., Leiva-García, R., García-Antón, J. *

Ingeniería Electroquímica y Corrosión (IEC). Departamento de Ingeniería Química y Nuclear. ETSI Industriales. Universitat Politècnica de València. Camino de Vera s/n, 46022 Valencia, Spain.

Tel. 34-96-387 76 32, Fax. 34-96-387 76 39, e-mail: jgarciaa@iqn.upv.es

This work studies the semiconducting behavior of passive films formed on AISI 316L in two different seawater solutions: non-polluted and polluted, collected from the volcano of El Hierro Island. Polarization measurements, potentiostatic passivation tests, electrochemical impedance spectroscopy and capacitance measurements were performed. Results show that the polluted seawater worsens passivation kinetics. Additionally, passive films formed on AISI 316L SS in polluted seawater have been found to be less protective than those formed in non-polluted seawater, showing a more defective structure owing to the acidity of the polluted medium.

Keywords: volcanic eruption; AISI 316L stainless steel; passive films; EIS; Mott-Schottky analysis.

Introduction

Last 10th of October of 2011 a volcano erupted in the Atlantic Ocean near the island of El Hierro (Canary Islands, Spain). When a volcano erupts in the sea, it releases gases and thermal water emissions, CO_2 being the main gas (90 %). This could cause a decrease of the seawater pH value and modify the behavior of the materials which are in contact with this medium[1-4].

Stainless steels (SS) are widely used in several industrial sectors. In particular, Austenitic stainless steels possess excellent resistance to general corrosion[5], especially AISI 316L stainless steel combines good mechanical properties and corrosion resistance due to the addition of molybdenum and low carbon content[6]. The high corrosion resistance of SS is related to the passive film formed on their surface. However, SS are susceptible to localized corrosive attacks, such as pitting corrosion, intergranular corrosion and stress corrosion cracking in highly electrical conducting media, such as seawater. Corrosion can cause great damages to marine steel infrastructures such as bridges, wharfs, platforms and pipeline systems[7]. These corrosion problems could be aggravated if the medium is altered, due to volcano emissions, since the resistance of the surface film is influenced by the pH[8].

There are some studies dealing with the passivation/corrosion processes of AISI 316L SS in natural seawater[9-11]. Mott–Schottky analysis is a powerful tool to study the semiconducting properties of passive films; some works have used this technique to evaluate passive film formed on AISI 316L stainless steels[12-14]. This work covers a

comprehensive study of the passivation/corrosion behavior of AISI 316L stainless steel which includes, among others, electrochemical impedance spectroscopy (EIS) and the Mott–Schottky analysis. The novelty of the study lies in the electrolyte used; that is polluted seawater collected from the volcano of El Hierro Island, since no works involving corrosion of SS in volcano seawater have been found in the literature. The main objective of this work is the study of the semiconducting behavior of passive films formed on AISI 316L in two different seawater solutions: non-polluted and polluted (collected from the volcano of El Hierro) seawater.

Experimental procedure

Materials, solution and electrochemical cell

Experiments were performed in non-polluted and polluted seawater. Figure 1 shows the coordinates where the seawater samples were taken on 19th of December of 2011. The polluted water was obtained on the focus of the volcano; the non-polluted samples were taken at enough distance to avoid the influence of the pollutants spread by the volcano, following the suggestions of the Spanish National Geographic Institute. Additionally, **Table 1** presents the main parameters of the non-polluted and polluted by the "El Hierro" volcano eruption seawaters. Moreover, composition of several metals was of the order of μg/l, in both seawaters. Aluminum, Zinc and Iron were the metals found in higher concentrations in the unpolluted seawater; especially, iron concentration could reach 1 mg/l. Prior to each experiment the pH and conductivity of the non-polluted and polluted seawater was measured. As shown in Table 1, the most substantial difference between both seawaters is pH.

The material tested was AISI 316L stainless steel (16.957 wt.% Cr, 10.171 wt.% Ni, 1.337 wt.% Mn, 2.298 wt.% Mo, 0.004 wt.% S, 0.368 wt.% Si, 0.030 wt.% P, 0.022 wt.% C, Bal. wt.% Fe). The electrodes were cylindrically shaped (8-mm in diameter and 55 mm long) and covered with a polytetrafluoroethylene (PTFE) coating. The area exposed to the solution was 0.5 cm^2. All specimens were wet abraded from 500 to 4000 SiC grit, and finally cleaned with ethanol, rinsed with distilled water and air-dried.

To perform the electrochemical tests a sheathed vertical electrochemical cell was used. The cell was made of glass and allows the introduction of three electrodes: a silver-silver chloride (Ag/AgCl 3M KCl) reference electrode, a platinum (Pt) wire as an auxiliary electrode and the working electrode, which was the AISI 316L SS. Electrochemical measurements were performed to AISI 316L stainless steel using an Autolab PGSTAT302N potentiostat, in both non-polluted and polluted seawater, at 25º C. In all cases the tests were repeated at least three times in order to verify reproducibility.

Polarization tests

Polarization tests began at a potential value of -250 $mV_{Ag/AgCl}$ with respect to the open circuit potential and the potential was subsequently scanned anodically until the current density reached 10 mA/cm^2, where the potential scan was reversed. A scan rate of 0.5 $mV \cdot s^{-1}$ was used.

Potentiostatic passivation tests

Before the passivation experiments, the electrode potential was kept at a cathodic value of -0.4 $V_{Ag/AgCl}$ for 15 minutes, to create reproducible initial conditions. Afterwards, the working electrode was polarized at the different formation potentials within the passive range of AISI 316L SS (from -100 $mV_{Ag/AgCl}$ to 150 $mV_{Ag/AgCl}$ in intervals of 50 mV) for 1 hour, in both non-polluted and polluted seawater at 25º C, to form a steady-state passive film. During passivation experiments, current density was recorded against time. Current density transients have been used to obtain the passivation time, t_r.

EIS and capacitance measurements

EIS and capacitance measurements were performed after passivation tests, once a stable passive film was formed on the surface of the samples. EIS measurements were conducted at the several formation potentials in the frequency range of 100 kHz-10 mHz, with a signal amplitude of 10 mV. Subsequently, the capacitance of the interface was calculated at a constant frequency of 5 kHz using a 10 mV amplitude signal and scanning the potential from the formation value in the negative direction at a rate of 25 mV s^{-1}. A high scanning rate was used to avoid electroreduction of the passive film and changes in film thickness during the measurements. At a sufficiently high scanning rate, the defect structure within the passive film is "frozen-in", to avoid the defect density from being affected by the change of the applied potential.

Results and discussion

Polarization tests

Figure 2 shows the cyclic polarization curves obtained in both seawater media. As tests were reproducible, the curves shown illustrate one of the recorded measurements. Cyclic polarization curves provide information about the corrosion, pitting, passivation and repassivation behavior of metals and alloys with parameters such as corrosion potential (E_{corr}), passivation current density (i_p), pitting potential (E_p) and repassivation potential (E_{rp}) (**Table 2**). According to the corrosion potential values determined from the curves, defined as the potential at which the net current density (sum of the anodic partial current density and the cathodic partial current density) was equal to zero, it can be observed that E_{corr} possesses more negative values in polluted seawater, indicating that AISI 316L SS becomes more active and is more likely to corrode in this medium. **Table 2** shows the passivation current densities obtained as the mean values where current density remains stable when potential shifts to the anodic direction. The i_p values determine the corrosion rates of the passive alloy. Current fluctuations appeared along the passive zone of the curves indicating metastable pitting before the pitting potential[15] (**Figure 2**). Passivation current densities significantly increase in polluted seawater, showing that its lower pH value affects the structure of the passive film. Pitting potentials (E_p) were determined as the potential at which current density reaches 100 $\mu A/cm^2$ [16]. Pitting potential indicates pitting corrosion susceptibility to local breakdown and stable pit initiation. AISI 316L SS is susceptible to pitting corrosion both in non-polluted and polluted seawater solutions, since chlorides are aggressive ions that promote passive film breakdown of stainless steel[16,17]. Pitting potential presents the most positive value in non-polluted solutions (**Table 2**), however, they are of the same magnitude order regardless the studied medium. E_{rp} was recorded at the crossing point between the backward and forward scans. This parameter refers to the limit below which the metal remains passive and active pits repassivate. If E_{rp} is more positive than

the corrosion potential, the material is able to regenerate an eventual breakdown of the passive film; however, if E_{rp} is more negative than the corrosion potential, the material is not able to completely repassivate the pits. The E_{rp} values obtained are more positive than the corrosion potential in all cases; thus, the material can repassivate the pits.

Potentiostatic passivation tests

Potentiostatic passivation tests were conducted in both non-polluted and polluted seawater at several formation potentials within the passive range of AISI 316L SS (see **Figure 2**). As a representative example, **Figure 3** shows the effect of the type of seawater (non-polluted and polluted) on the current density transients of AISI 316L SS when its potential stepped from the cathodic cleaning potential of -0.4 $V_{Ag/AgCl}$ to the formation potential of -0.1 $V_{Ag/AgCl}$. Regardless of the type of seawater, the passive current density of AISI 316L SS decreases exponentially with passivation time as the passive film grows on the electrode surface, and eventually reaches a very low steady-state value (i_{ss}) after 1 hour of passivation. During the first 100 seconds of the test, current density values are significantly higher in the sample immersed in the polluted seawater than in the sample immersed in the non-polluted seawater (**Figure 3**). The main difference between both samples is the current density peak recorded immediately after the potential step, which is far higher in the sample immersed in polluter seawater.

The passivation rate of a metal or alloy can be compared in terms of the time required to achieve a predetermined degree of passivation after stepping the potential from the cathodic cleaning potential to the formation potential, which is known as passivation

time (t_p)[18,19]. The shorter the passivation time, the faster the passivation rate of an alloy will be. Taking an arbitrary value of passive current density of i_r = 0.5 μA/cm^2, similar to the values of passive current density obtained from the polarization curves (**Figure 2**), passivation time can be determined from **Figure 3** in both non-polluted and polluted seawater at a formation potential of -0.1 $V_{Ag/AgCl}$. Passivation time values, t_p, were 218 and 457 s, respectively, showing a 109.63% increase of t_p in the polluted seawater with respect to the value in the non-polluted seawater at an applied formation potential of -0.1 $V_{Ag/AgCl}$. It can be observed that the value of t_p in the polluted seawater is more than two times higher than in the non-polluted seawater. Therefore, passivation is slower in the sample immersed in the polluted seawater.

EIS measurements

Electrochemical impedance spectra were measured at different formation potentials in the passive region (see polarization curves in **Figure 2**). By way of illustration, Nyquist and Bode plots are shown in **Figure 4** for AISI 316L SS in both polluted and non-polluted seawater, at a formation potential of -100 $mV_{Ag/AgCl}$ and 25º C. It can be observed that the AISI 316L SS electrode immersed in the non-polluted seawater has higher Faradic impedance than the electrode immersed in the polluted seawater. In Bode plots, a non-ideal capacitive behaviour is observed in both electrolytes.

The stability of the system is crucial for the validity of EIS measurements. An independent check of the validity of impedance data (that is, compliance of the system with the constraints of the Linear Systems Theory (LST)) is possible through the use of Kramers–Kronig (K–K) transforms. The Kramers–Kronig transforms have been applied

to the experimental impedance data by transforming the real axis into the imaginary axis and the imaginary axis into the real axis and then comparing the transformed quantities with the respective experimental data. Typical Kramers–Kronig transforms of the impedance data obtained in the present study for AISI 316L SS in both non-polluted and polluted seawater at a formation potential of -0.1 $V_{Ag/AgCl}$ are displayed in **Figure 5**. It can be seen that the K-K transforms are almost exact, following the same tendency as the experimental values. The success of the K–K transforms demonstrates that the system (AISI 316L/seawater) remained stable during the measurement time, is causal and is linear. These conditions are prerequisites for the analysis of the data in terms of electrical analogues.

The equivalent electric circuit used to interpret EIS spectra of anodically formed passive films is shown in **Figure 6**. In this equivalent circuit, R_S represents the electrolyte resistance, R_1 and CPE_1 correspond to the charge transfer resistance and the capacitance of the passive film/electrolyte interface, respectively, and Z_W is a Warburg component, which has been used to interpret the transport of vacancies within the passive film, in the frame of the Point Defect Model[20-23]. The Warburg impedance is represented by means of an Open-Boundary Finite Length Diffusion element (OFLD element)[22,24-26], which models dimensional diffusion through a layer of finite thickness with absorbing boundary condition. The equation of the OFLD element is the following[24-26]:

$$Z_W(OFLD) = \frac{\tanh\left(B \cdot \sqrt{j\omega}\right)}{Y_0 \cdot \sqrt{j\omega}} \qquad \textbf{(1)}$$

Where j = $(-1)^{1/2}$, $B = \delta/(D)^{1/2}$, D is the diffusion coefficient of vacancies, δ is the diffusion layer thickness, $Y_0 = (\sigma(2)^{1/2})^{-1}$ and σ is the Warburg coefficient, which is inversely proportional to the vacancy density within the passive film[22,27].

A constant-phase element (CPE) representing a shift from the ideal capacitor has been used instead of the capacitance itself. The impedance of a constant-phase element is defined as:

$$Q = Z_{CPE} = \left[C(j\omega)^{\alpha}\right]^{-1} \quad \textbf{(2)}$$

where α, defined as a CPE power, is an adjustable parameter that lies between -1 and 1. For α = 1 the CPE describes an ideal capacitor, and for α = 0 the CPE is an ideal resistor. When α = 0.5 the CPE represents a Warburg impedance with diffusional character and for 0.5 < α < 1 the CPE describes a frequency dispersion of time constants due to local heterogeneities in the dielectric material. A pure inductance yields α = -1.

The CPE used in the equivalent electric circuit of **Figure 6** has been converted into a pure capacitance (C) by means of the following equation[28,29]:

$$C = Q^{1/n}\left(R_S^{-1} + R_1^{-1}\right)^{(n-1)/n} \quad \textbf{(3)}$$

where $Q = Z_{CPE}$ (eq. (2)).

The parameters of the equivalent circuit of **Figure 6** obtained from the fitting procedure are shown in **Table 3**. The charge transfer resistance, R_1, is always higher in the non-polluted seawater, which reflects better protective properties of the passive films. Thus,

the charge transfer reactions which take place at the AISI 316L SS electrodes surface are enhanced in the polluted seawater. On the other hand, the values of the interfacial capacitance, C_1, are higher in the polluted seawater, which suggests, along with the decrease of the charge transfer resistance R_1, worse protective properties of the passive films formed on AISI 316L SS. Finally, Warburg coefficient values are always lower in the polluted seawater, which indicates an increase in the number of point defects within the passive films formed in this seawater.

Regarding the influence of formation potential on the impedance response of passive films formed on AISI 316L SS, it can be observed from **Table 3** that R_1 increases and C_1 decreases with increasing formation potentials. These results indicate that passive films formed at higher passive potentials are more protective than those formed at lower potentials within the passive region. According to the increasing values of the Warburg coefficient with increasing formation potentials, the improvement of the protective properties of passive films formed at higher passive potentials is related to a decrease in the number of point defects within their structure.

Capacitance results

The electrochemical capacitance of the passive film/electrolyte interface was measured as a function of the applied potential to assess the semiconductive properties of the passive films. Since the space charge region developed in the passive film and the Helmholtz layer can be considered as two capacitors in series, the measured capacitance of the film/electrolyte interface can be written as[30,31]:

$$\frac{1}{C} = \frac{1}{C_{SC}} + \frac{1}{C_H} \quad \textbf{(4)}$$

where C_{SC} is the capacitance of the space charge layer and C_H the capacitance of the Helmholtz layer.

Figure 7 shows the capacitance-potential relationship after the formation of the film at 0 $V_{Ag/AgCl}$ on the AISI 316L SS surface in the non-polluted seawater for 1 hour. This curve is representative of the results obtained at the different applied potentials in both polluted and non-polluted seawater. Below 0 $V_{Ag/AgCl}$, the capacitance starts rising as a consequence of the reduction of the space charge layer thickness, reaching a maximum value of 33.2 μF/cm^2 at a potential between -0.50 and -0.55 $V_{Ag/AgCl}$. In this narrow region of potentials the contribution of the space charge layer to the measured capacitance is limited and the Helmholtz layer dominates the capacitance response. At potentials more negative than -0.55 $V_{Ag/AgCl}$ capacitance values decrease as the space charge layer thickness increases.

It is important to remark that capacitance is frequency dependant[32-35]. Several causes for the frequency dispersion have been proposed: (i) a non-uniform distribution of point defects through the passive film[33,35]; (ii) the contribution of surface states to the capacitance response (adsorption of anions, e.g. chlorides, or other species) [33,35]; (iii) the ionic part of the space charge layer, which gives a contribution only at low frequencies due to the low ionic mobility, particularly in heavily doped materials where the space charge region is very thin (passive films generally satisfy these requirements) [33,34,36]; (iv) dielectric relaxation phenomena which occur throughout the space charge layer and

the Helmholtz layer[31-33,35,36]; (v) an amorphous and strongly disordered semiconductor nature of passive films, characterized by a high density of localized states between the valence and the conduction band and whose charging leads to a strong frequency dependent capacitance behaviour[33,36]; (vi) presence of deep donor states[32,33,36].

Figure 8 shows the capacitance-potential curves obtained for AISI 316L SS at a formation potential of 0 $V_{Ag/AgCl}$, at different frequencies in the non-polluted seawater. It can be observed that there is a strong frequency dependence at low frequencies (capacitance curves shift to higher values with decreasing frequencies), but the capacitance becomes almost independent of frequency at approximately 5 kHz. Therefore, a value of 5 kHz has been used in this work as the applied frequency to eliminate capacitance dependence on frequency.

Presented as the Mott-Schottky relation, eq. (4) becomes:

$$\frac{1}{C^2} = \frac{1}{C_{SC}^2} + \frac{1}{C_H^2} + \frac{2}{C_{SC}C_H} \quad \textbf{(5)}$$

It is usually assumed that the Helmholtz layer capacitance is so large compared with the space charge layer capacitance that the total capacitance measured can be treated as the space charge layer capacitance and the potential drop caused by the applied potential occurs entirely within the space charge region. However, several studies[30,37] have shown that a significant part of the potential difference at the semiconductor/electrolyte interface extends to the Helmholtz layer in the solution. Therefore, C_H should not be neglected, particularly at highly doped semiconductors, such as passive films[30,31]. In this

case, the passive film/electrolyte interface can be described by the following expressions[30,31,33]:

$$\frac{1}{C^2} = \frac{1}{C_H^2} + \frac{2}{\varepsilon\varepsilon_0 e N_D}\left(E - E_{FB} - \frac{kT}{e}\right) \qquad \textbf{\textit{n}-type} \qquad \textbf{(6a)}$$

$$\frac{1}{C^2} = \frac{1}{C_H^2} - \frac{2}{\varepsilon\varepsilon_0 e N_A}\left(E - E_{FB} - \frac{kT}{e}\right) \qquad \textbf{\textit{p}-type} \qquad \textbf{(6b)}$$

where ε is the dielectric constant of the passive film (a value of 15.6 has been assumed for the chromium and iron oxides formed on austenitic stainless steels[33]), ε_0 is the vacuum permittivity ($8.85 \cdot 10^{-14}$ F/cm), e is the electron charge ($1.60 \cdot 10^{-19}$ C), N_D and N_A are respectively the donor and acceptor densities, E_{FB} is the flat-band potential k is the Boltzmann constant ($1.38 \cdot 10^{-23}$ J/K) and T is the absolute temperature.

Figure 9 shows the plot of C^{-2} vs. applied potential, E, for the films formed on AISI 316L SS at different potentials in both polluted and non-polluted seawater for 1 hour. Mott-Schottky plots reveal the existence of two regions where a Mott-Schottky type behavior can be observed (straight lines at low and high potentials), separated by the flat-band potential E_{FB}. In the more anodic of these two regions (E > -0.4 V for non-polluted seawater and E > -0.25 V for polluted seawater, **Figures 9a** and 9**b**, respectively) the capacitance results can be interpreted as representative of the behavior of an *n*-type semiconductor. In the second potential region (E < -0.7 V for non-polluted seawater and E < -0.5 V for polluted seawater), the negative slopes of the straight lines illustrate the electrochemical behavior of a *p*-type semiconductor.

According to Hakiki et al.[31] the electronic structure of the passive films formed on stainless steels can be described by a bilayer model composed of a *n*-type outer region of iron oxide (Fe_2O_3) and hydroxide near the solutions, and a *p*-type inner region of chromium oxide (Cr_2O_3) near the metal. Tsuchiya et al.[38] have also used a bilayer model to describe the semiconducting behavior of passive films formed on Fe-Cr alloys in sulphuric acid solutions, assuming that these passive films were composed of an outer *n*-type hydroxide layer $Cr(OH)_3$ and an inner *p*-type oxide layer of Cr_2O_3. However, the bilayer structure of passive films formed on stainless steels has been demonstrated to be more complex[8,39-42]. The *n*-type outer region would be enriched in Fe^{3+} species, such as Fe_2O_3, FeO(OH) and $Fe(OH)_3$, as well as $Cr(OH)_3$ and CrO(OH). The *p*-type inner region would consist of an anhydrous mixed Fe-Cr oxide, most probably with a spinel structure, e.g. $FeCr_2O_4$ (chromite)[39]. This spinel should be enriched in Cr, with the octahedral sites preferentially occupied by Cr(III)[8,40], or even Fe(III)[39], so its structure should be represented in a more accurate formula as $Fe(II)[Cr(III)_xFe(III)_{(1-x)}]_2O_4$, where $0 < x \leq 1$ [39]. Nickel may also replace iron and chromium in the spinel[8].

The $1/C^2$ vs. E plots shown in **Figure 9** exhibit a minimum in the flat-band potential region. Therefore, the capacitance should not be derived from a single space charge region, but from at least two regions[47]. In a metal/film/electrolyte system, space charge regions can be formed in the film either at the film/electrolyte interface or at the metal/film interface[55].

From Mott-Schottky diagrams, the system can be divided into three interfaces: (I) metal/inner layer; (II) inner layer/outer layer; (III) outer layer/electrolyte. **Figure 10** shows a schematic representation of the energy-band model corresponding to the

behavior observed. At interfaces (I) and (III), two space charge regions develop in the inner and outer layers, respectively, depending on the applied potential. At potentials more positive than the flat-band potential (E_{FB}), the conduction and valence bands bend upwards at the outer layer/electrolyte interface (III), promoting the development of a depletion space charge region, while there is an accumulation of holes at interface (I), which behaves as an ohmic contact. On the contrary, at potentials more negative than E_{FB}, the bands bend downwards and the situation previously described is reversed. Thus, at the outer layer/electrolyte interface (III) an accumulation of electrons occurs, with a consequent ohmic behavior of the outer layer of the film, which converts from a semiconductor to a metal-like conductor. Therefore, the capacitance measurements performed in the potential region $E < E_{FB}$ reflect the semiconducting properties of the inner layer of the passive film. According to this model of the electronic structure of the passive film formed on AISI 316L SS, the film behaves as a *p-n* heterojunction where the space charge regions are not in contact with each other, but localized at the interfaces (I) and (III).

From the slopes of the linear zones in **Figure 9**, donor and acceptor densities (N_D and N_A) can be calculated for *n*-type and *p*-type semiconductors using equations (6a) and (6b), respectively. For stainless steels, the predominant acceptor species in *p*-type layers are chromium vacancies, $V_{Cr}^{3'}$, whereas donor species in *n*-type layer are oxygen vacancies, $V_O^{\bullet\bullet}$ and/or cation interstitials[44-46]. **Table 4** shows the values of N_A and N_D for AISI 316L SS in both polluted and non-polluted seawater at the different formation potentials.

It can be seen from **Table 4** that N_D and N_A values are of the order of 10^{20}, according to the results of other authors for stainless steels[40,47,48]. Regardless of the type of seawater, defect densities decrease as passive film formation potential increases, since anodic polarization has an annealing effect which eliminates some defects in the passive film[49]. Thus, passive films formed at lower passive potentials on AISI 316L SS in both polluted and non-polluted seawater have more disordered structures and higher defect densities than those formed at higher passive potentials. These results confirm the explanations given above concerning the increasing values of the Warburg coefficient with increasing formation potentials (**Table 3**).

Regarding the effect of the type of seawater on the defect structure of the passive films formed on AISI 316L SS electrodes, both *p*-type inner layer and *n*-type outer layer are more defective for passive films formed in the polluted seawater, since N_D and N_A values are higher than in the non-polluted seawater (**Table 4**). The higher values of N_D in the polluted seawater are related to its higher acidity, since H^+ (acceptor species[35]) would adsorb at the film/electrolyte interface and react with the oxygen present in the passive film, generating increasingly anionic oxygen vacancies[35].

According to the Point Defect Model (PDM)[23,50] aggressive anions such as halides can adsorb in surface oxygen vacancies, which leads to the generation of a cation vacancy/oxygen vacancy via a Schottky pair type of reaction. The oxygen vacancies in turn react with additional anions (chloride in the present case) at the film/electrolyte interface to generate more cation vacancies, in an autocatalytic process which eventually could result in passivity breakdown due to the thinning of the passive film, or the local detachment from the metal. Therefore, the donor density N_D characterizes the

affinity of aggressive anions (i.e. chlorides) for the passive film. The fact that the passive film formed in the polluted seawater is more donor-doped than that formed in the non-polluted seawater reveals then a larger sensitivity to pit nucleation related to an easier incorporation of chloride anions in the oxygen vacancies present in the outer layer of the passive film. However, the pitting potential values, E_p, recorded in both seawater media (**Table 2**) are of the same magnitude order. Thus, the defect density values might not have a considerable influence on the pitting corrosion behavior of the AISI 316L SS.

According to the results obtained in the Mott-Schottky analysis and to the proposed model for the electronic structure of the passive film formed on AISI 316L SS (**Figure 10)**, two space charge regions appear at the metal/inner layer and outer layer/electrolyte interfaces. From the measured capacitance values, the capacitance of these space charge regions, C_{SC}, can be obtained using eq. (4). As it has been explained above, the capacitances of the Helmholtz layer, C_H, should not be neglected. It can be assumed that at the flat-band potential, the total measured capacitance is equal to the electrical double layer capacitance, C_{dl}, since no depletion layer exists at this potential and the contribution of the space charge or the passive film to the total capacitance values is negligible[34,35]. Thus, C_{dl} values were estimated to be about 20-40 μF cm^{-2}, depending on the seawater and the applied potential, and can be assumed to be mainly due to the Helmholtz layer. The capacitance of the electrical double layer, C_{dl}, is made up of two components[51,52]:

$$\frac{1}{C_{dl}} = \frac{1}{C_H} + \frac{1}{C_D} \qquad \textbf{(7)}$$

where C_H corresponds to the capacitance of the Helmholtz layer and C_D is the capacitance of the diffuse charge or Guoy-Chapman capacitance. The value of C_{dl} is therefore governed by the smaller of the two components. In sufficiently concentrated solutions or even at large polarizations in dilute media, C_D becomes so large that it no longer contributes to C_{dl} and the capacity of the electrical double layer is effectively equal to the capacitance of the Helmholtz layer[51,52]. Thus, in seawater and working at potentials within the passive range, it can be assumed that $C_{dl} \approx C_H$.

The maximum thickness of the space charge layers formed in both inner and outer regions of the passive films can be calculated from the C_{SC} values determined at those two potentials where $1/C^2$ reaches a maximum in the Mott-Schottky plots, that is, at the formation potential (thickness of the outer layer) and at the most negative potential (thickness of the inner layer). Thicknesses have been calculated with the formula for a parallel plane condenser[34,53]:

$$C_{SC} = \frac{\varepsilon \cdot \varepsilon_0}{W} \qquad \textbf{(8)}$$

where W is the space charge layer thickness. **Table 5** gives the thickness values of the space charge layers formed on the two regions of the passive film (inner *p*-type layer and outer *n*-type layer, W_i and W_o, respectively) for AISI 316L SS in both polluted and non-polluted seawater. The magnitude of the thickness of the space charge layers shown in **Table 5** are in good agreement with the thickness of passive films formed on stainless steels, which is in the range of 1-3 nm[50]. Thus, the steady-state thickness of the passive film, L_{SS}, can be estimated from the sum of W_i and W_o.

In general, the thickness of the outer layer decreases in the polluted seawater, whereas the inner layer is thicker in this seawater at low formation potentials. This fact could be explained from the lower pH value of the polluted seawater. It has been reported that at low pH values, passive films formed on stainless steels become enriched in chromium, observing an increase in the thickness of the inner layer[8]. On the other hand, a decrease in pH enhances the dissolution rate of iron oxides and hydroxides present in the outer layer of the passive film[8]. Nevertheless, the increase of the thickness of the inner layer in the polluted seawater at low formation potentials due to the decrease of pH does not imply an improvement of protective properties of the passive film, since passive films formed in this seawater have been demonstrated to be less resistant and to have a more defective structure. Therefore, the thickness of the oxide layers that form the passive film should not be related directly with their protective properties, as other authors have indicated[44], being the semiconducting properties and the defect structure of the passive film the fundamental factors to evaluate its corrosion resistance.

The influence of the formation potential on both inner and outer layers regions of the passive film can also be observed in **Table 5**. On the whole, the thickness of both layers increases with increasing formation potentials. **Figure 11** shows a linear relationship between the estimated steady-state thickness of the passive film, L_{SS}, and the formation potential for both polluted and non-polluted seawater. This linear dependence between L_{SS} and E is a well established experimental result in the anodic oxidation of metals[23,50].

Determination of the diffusivity of point defects

Several authors have demonstrated that the diffusivity of donor species (oxygen vacancies and/or cation interstitials) through the passive film, N_D, decreases exponentially as the formation potential increases[12,46,54,55]. It has been proved that the relationship between the donor density and the film formation potential can be described as[54]:

$$N_D = \omega_1 \exp(-bE) + \omega_2 \quad \textbf{(9)}$$

where ω_1, ω_2 and b are unknown constants that can be determined experimentally. The donor density, N_D, has already been determined from Mott-Schottky analysis (**Table 4**).

According to the Point Defect Model (PDM)[23,50,56], the flux of oxygen vacancies and/or cation interstitials through the passive film is essential to the film growth process. Sikora et. al.[54] demonstrated that ω_2 in eq. (9) could be related to the diffusivity of point defects D_O by the following equation based on the Nernst-Plank transport equation:

$$D_O = -\frac{J_O RT}{2F\omega_2 \varepsilon_L} \quad \textbf{(10)}$$

where J_o is the steady state flux of donors, F the Faraday constant, ε_L is the mean electric field strength, R is the gas constant and T is absolute temperature. However, Bojinov[57] pointed out that eq. (10) was a special case of general vacancy motion equation with a low field approximation. With a high field approximation, which is more appropriate to the case of passive films, the donor diffusivity within the passive film can be calculated by using:

$$D_O = -\frac{2aJ_O}{\omega_2 \exp\left(2aF\varepsilon_L / RT\right)} \quad \textbf{(11)}$$

where a is the half jump distance ($5 \cdot 10^{-8}$ cm for steels[58,59]). Thus, eqs. (9) and (11) will be used in this work to calculate D_O in the passive film of AISI 316L SS, instead of eq. (10), assuming a mean value of 1.8×10^6 V cm^{-1} for ε_L, which is consistent with the values found in the literature for Fe, Fe-Cr and Fe-Cr-Ni alloys in neuter and slightly alkaline solutions[60].

The steady state flux of point defects, J_O, can be expressed in terms of steady state current density through the passive film[54]:

$$J_O = -\frac{i_{SS}}{2e} \quad \textbf{(12)}$$

where e is the charge of an electron (1.602×10^{-19} C) and i_{ss} is the mean steady-state passive current density obtained at the end of the potentiostatic tests (0.0595 μA cm^{-2} for the non-polluted seawater, and 0.0752 μA cm^{-2} for the polluted seawater).

The donor density, N_D, is presented in **Figure 12** as a function of formation potential for AISI 316L SS in both polluted and non-polluted seawater, in order to determine diffusivities of point defects. The values of D_O obtained from eq. (11) are $5.70 \cdot 10^{-19}$ cm^2 s^{-1} for the non-polluted seawater and $1.92 \cdot 10^{-19}$ cm^2 s^{-1} for the polluted seawater. Since the main difference between both seawaters is pH (**Table 1**), it can be said that the decrease of pH in the polluted seawater has little effect on the diffusivity of point

defects within the passive film formed on AISI 316L SS surface. Other authors have also observed small variations of D_O values at different pH[12]. Thus, the diffusivities of the point defects within the passive film formed in both seawaters are in the same range of 10^{-19} cm^2 s^{-1}, although it has been demonstrated by Mott-Schottky analysis that defect densities, N_D and N_A, increase in the polluted seawater.

4. CONCLUSIONS

The parameters obtained from the polarization curves indicate better protective properties of AISI 316L in non-polluted solutions due to its more noble corrosion potential and passivation current densities. Repassivation potentials show that AISI 316L SS could repassivate an eventual breakdown of the passive film in both studied media.

The passivation current density in the polluted sea water has been found to be more than twice the passivation current density in the non-polluted seawater. Hence, passivation kinetics is negatively affected by the composition of the polluted seawater.

The decrease of the charge transfer resistance, R_1, along with the increase of the interfacial capacitance, C_1, indicate worse protective properties of passive films formed on AISI 316L SS in the polluted seawater. Furthermore, Warburg coefficient values are always lower in the polluted seawater, which indicates an increase in the number of point defects within the passive films formed in this seawater.

Mott-Schottky plots for AISI 316L SS in both seawater media reveal the existence of two regions where a Mott-Schottky type behavior can be observed (*n*-type semiconductor at potentials higher than E_{FB} and *p*-type semiconductor at potentials lower than E_{FB}). These results can be explained considering a bilayer model of the passive film, with a *n*-type outer region enriched in Fe^{3+} species, such as Fe_2O_3, FeO(OH) and $Fe(OH)_3$, as well as $Cr(OH)_3$ and CrO(OH), and a *p*-type inner region made up of an anhydrous mixed Fe-Cr oxide, most probably with a spinel structure.

The density of point defects within the passive films of AISI 316L SS formed in the polluted seawater is higher than in the non-polluted seawater, both in the *p*-type inner layer and *n*-type outer layer. These results are closely related to the higher acidity of polluted seawater since the adsorption of H^+ at the film/electrolyte interface generates additional oxygen vacancies.

The more defective structure of the passive film formed in the polluted seawater reveals a larger sensitivity to pit nucleation, related to an easier incorporation of chloride anions in the oxygen vacancies present in the outer layer of the passive film, in agreement with the postulates of the Point Defect Model.

ACKNOWLEDGEMENTS

We wish to express our gratitude to Prof. Dr. Aurora Santos López, Dr. Rosario Lunar Hernández and Dr. Jose Arnoso Sampedro (Instituto de Geociencias (CSIC, UCM)), Dr. Carmen López Moreno (Head of the Volcano Monitoring Unit, Spanish National Geographic Institute), Humberto Gutiérrez García (Head of the Civil Protection and

Emergency Management Service of the General Directorate of Security and Emergencies of the Canary Islands) and Alejandro Ramos Fenández (Coordinador Multisectorial del Centro Coordinador de Emergencias 1-1-2 del Gobierno de Canarias) for their help in supplying both non-polluted and polluted seawater samples, to the UPV CEI 2011 and to Dr. M. Asunción Jaime for her translation assistance.

REFERENCES

[1] G. Chiodini, S. Caliro, G. Caramanna, D. Granieri, C. Minopoli, R. Moretti, L. Perotta, G. Ventura. Geochemistry of the Submarine Gaseous Emissions of Panarea (Aeolian Islands, Southern Italy): Magmatic vs. Hydrothermal Origin and Implications for Volcanic Surveillance, Pure Appl. Geophys. 163 (2006) 759-780.

[2] A. Esposito, G. Giordano, M. Anzidei. The 2002-2003 submarine gas eruption at Panarea volcano (Aeolian Islands, Italy): Volcanology of the seafloor and implications for the hazard scenario, Mar. Geol. 227 (2006) 119-134.

[3] P. Sedwick, D. Stuben. Chemistry of shallow submarine warm springs in an arc-volcanic setting: Vulcano Island, Aeolian Archipelago, Italy, Mar. Chem. 53 (1996) 147-161.

[4] C. Siebe, J. C. Komorowski, C. Navarro, J. McHone, H. Delgado, A. Cortés. Submarine eruption near Socorro Island, Mexico: Geochemistry and scanning electron microscopy studies of floating scoria and reticulite, J. Volcanol. Geoth. Res. 68 (1995) 239-271.

[5] B. T. Lu, Z. K. Chen, J. L. Luo, B. M. Patchett, Z. H. Xu. Pitting and stress corrosion cracking behavior in welded austenitic stainless steel, Electrochim. Acta 50 (2005) 1391-1403.

[6] J. Oñoro. Corrosion fatigue behavior of 317LN austenitic stainless steel in phosphoric acid, Int. J. Pres. Ves. Pip. 86 (2009) 656-660.

[7] J. Duan, S. Wu, X. Zhang, G. Huang, M. Du, B. Hou. Corrosion of carbon steel influenced by anaerobic biofilm in natural seawater, Electrochim. Acta 54 (2008) 22-28.

[8] L. Freire, M. J. Carmezim, M. G. S. Ferreira, M. F. Montemor. The passive behavior of AISI 316 in alkaline media and the effect of pH: A combined electrochemical and analytical study, Electrochim. Acta 55 (2010) 6174-6181.

[9] N. Le Bozec, C. Compère, M. L'Her, A. Laouenan, D. Costa, P. Marcus. Influence of stainless steel surface treatment on the oxygen reduction reaction in seawater, Corros. Sci. 43 (2001) 765-786.

[10] A. Al Odwani, M. Al-Tabtabaei, A. bdel-Nabi. Performance of high chromium stainless steels and titanium alloys in Arabian Gulf seawater, Desalination 120 (1998) 73-81.

[11] S. A. Al-Fozan, A. U. Malik. Effect of seawater level on corrosion behavior of different alloys, Desalination 228 (2008) 61-67.

[12] A. Fattah-alhosseini, M. A. Golozar, A. Saatchi, K. Raeissi. Effect of solution concentration on semiconducting properties of passive films formed on austenitic stainless steels, Corros. Sci. 52 (2010) 205-209.

[13] A. Fattah-alhosseini, F. Soltani, F. Shirsalimi, B. Ezadi, N. Attarzadeh. The semiconducting properties of passive films formed on AISI 316 L and AISI 321 stainless steels: A test of the point defect model (PDM), Corros. Sci. 53 (2011) 3186-3192.

[14] E. C. Paredes, A. Bautista, S. M. Alvarez, F. Velasco. Influence of the forming process of corrugated stainless steels on their corrosion behavior in simulated pore solutions, Corros. Sci. 58 (2012) 52-61.

[15] R. C. Newman. 2001 W.R. Whitney Award Lecture: Understanding the Corrosion of Stainless Steel, CORROSION 57 (2001) 1030-1041.

[16] M. Kaneko, H. S. Isaacs. Pitting of stainless steel in bromide, chloride and bromide/chloride solutions, Corros. Sci. 42 (2000) 67-78.

[17] M. Kaneko, H. S. Isaacs. Effects of molybdenum on the pitting of ferritic- and austenitic-stainless steels in bromide and chloride solutions, Corros. Sci. 44 (2002) 1825-1834.

[18] S. Ahila, B. Reynders, H. J. Grabke. The evaluation of the repassivation tendency of Cr-Mn and Cr-Ni steels using scratch technique, Corros. Sci. 38 (1996) 1991-2005.

[19] H. S. Kwon, E. A. Cho, A. Yeom. Prediction of Stress Corrosion Cracking Susceptibility of Stainless Steels Based on Repassivation Kinetics, CORROSION 56 (2000) 32-40.

[20] C. Y. Chao, L. F. Lin, D. D. Macdonald. A Point Defect Model for Anodic Passive Films III. Impedance Response, J. Electrochem. Soc. 129 (1982) 1874-1879.

[21] D. D. Macdonald, R. Y. Liang, B. G. Pound. An Electrochemical Impedance Study of the Passive Film on Single Crystal Ni(111) in Phosphate Solutions, J. Electroch. Soc. 134 (1987) 2981-2986.

[22] M. Sánchez, J. Gregori, M. C. Alonso, J. J. García-Jareño, F. Vicente. Anodic growth of passive layers on steel rebars in an alkaline medium simulating the concrete pores, Electrochim. Acta 52 (2006) 47-53.

[23] D. D. Macdonald. The Point Defect Model for the Passive State, J. Electrochem. Soc. 139 (1992) 3434-3449.

[24] I. D. Raistrick, D. R. Franceschetti, J. R. Macdonald, E. Barsoukov, J. R. Macdonald (eds.), Impedance Spectroscopy. Theory, Experiment, and Applications, 2005.

[25] Z. Grubac, Z. Petrovic, J. Katic, M. Metikos-Hukovic, R. Babic. The electrochemical behavior of nanocrystalline nickel: A comparison with polycrystalline nickel under the same experimental condition, J. Electroanal. Chem. 645 (2010) 87-93.

[26] F. Mansfeld, L. T. Han, C. C. Lee, G. Zhang. Evaluation of corrosion protection by polymer coatings using electrochemical impedance spectroscopy and noise analysis, Electrochim. Acta 43 (1998) 2933-2945.

[27] Z. Grubac, M. Metikos-Hukovic. EIS study of solid-state transformations in the passivation process of bismuth in sulfide solution, J. Electroanal. Chem. 565 (2004) 85-94.

[28] C. Valero Vidal, A. Igual-Muñoz. Study of the adsorption process of bovine serum albumin on passivated surfaces of CoCrMo biomedical alloy, Electrochim. Acta 55 (2010) 8445-8452.

[29] B. Hirschorn, M. E. Orazem, B. Tribollet, V. Vivier, I. Frateur, M. Musiani. Determination on effective capacitance and film thickness from constant-phase-element parameters. Electrochim. Acta 55 (2010) 6218-6227.

[30] K. Uosaki, H. Kita. Effects of the Helmholtz Layer Capacitance on the Potential Distribution at Semiconductor/Electrolyte Interface and the Linearity of the Mott-Schottky Plot, J. Electrochem. Soc. 130 (1983) 895-897.

[31] N. B. Hakiki, S. Boudin, B. Rondot, M. Da Cunha Belo. The electronic structure of passive films formed on stainless steels, Corros. Sci. 37 (1995) 1809-1822.

[32] W. P. Gomes, D. Vanmaekelbergh. Impedance spectroscopy at semiconductor electrodes: Review and recent developments, Electrochim. Acta 41 (1996) 967-973.

[33] A. D. Paola. Semiconducting properties of passive films on stainless steels, Electrochim. Acta 34 (1989) 203-210.

[34] M. Da Cunha Belo, N. E. Hakiki, M. G. S. Ferreira. Semiconducting properties of passive films formed on nickel-base alloys type Alloy 600: influence of the alloying elements, Electrochim. Acta 44 (1999) 2473-2481.

[35] J. Amri, T. Souier, B. Malki, B. Baroux. Effect of the final annealing of cold rolled stainless steels sheets on the electronic properties and pit nucleation resistance of passive films, Corros. Sci. 50 (2008) 431-435.

[36] L. Hamadou, A. Kadri, N. Benbrahim. Characterisation of passive films formed on low carbon steel in borate buffer solution (pH 9.2) by electrochemical impedance spectroscopy, Appl. Surf. Sci. 252 (2005) 1510-1519.

[37] J. O. Bockris. Interfacial electron transfer as a significant step in photoelectrochemical reactions on some semiconductors, J. Appl. Phys. 52 (1981) 808-810.

[38] H. Tsuchiya, S. Fujimoto, O. Chihara, T. Shibata. Semiconductive behavior of passive films formed on pure Cr and Fe-Cr alloys in sulfuric acid solution, Electrochim. Acta 47 (2002) 4357-4366.

[39] T. L. S. Wijesinghe, D. J. Blackwood. Characterisation of passive films on 300 series stainless steels, Appl. Surf. Sci. 253 (2006) 1006-1009.

[40] M. J. Carmezim, A. M. P. Simoes, M. F. Montemor, M. Da Cunha Belo. Capacitance behavior of passive films on ferritic and austenitic stainless steel, Corros. Sci. 47 (2005) 581-591.

[41] M. Da Cunha Belo, B. Rondot, C. Compere, M. F. Montemor, A. M. P. Simoes, M. G. S. Ferreira. Chemical composition and semiconducting behavior of stainless steel passive films in contact with artificial seawater, Corros. Sci. 40 (1998) 481-494.

[42] G. Lothongkum, S. Chaikittisilp, A. W. Lothongkum. XPS investigation of surface films on high Cr-Ni ferritic and austenitic stainless steels, Appl. Surf. Sci. 218 (2003) 203-210.

[43] A. Goossens, M. Vazquez, D. D. Macdonald. The nature of electronic states in anodic zirconium oxide films part 1: The potential distribution, Electrochim. Acta 41 (1996) 35-45.

[44] A. Shahryari, S. Omanovic. Improvement of pitting corrosion resistance of a biomedical grade 316LVM stainless steel by electrochemical modification of the passive film semiconducting properties, Electrochem. Commun. 9 (2007) 76-82.

[45] Y. X. Qiao, Y. G. Zheng, W. Ke, P. C. Okafor. Electrochemical behavior of high nitrogen stainless steel in acidic solutions, Corros. Sci. 51 (2009) 979-986.

[46] M. Metikos-Hukovic, R. Babic, Z. Grubac, Z. Petrovic, N. Lajçi. High corrosion resistance of austenitic stainless steel alloyed with nitrogen in an acid solution, Corros. Sci. 53 (2011) 2176-2183.

[47] N. E. Hakiki, M. Da Cunha Belo, A. M. P. Simoes, M. G. S. Ferreira. Semiconducting Properties of Passive Films Formed on Stainless Steels, J. Electrochem. Soc. 145 (1998) 3821-3829.

[48] L. Pons, M. L. Délia, R. Basséguy, A. Bergel. Effect of the semi-conductive properties of the passive layer on the current provided by stainless steel microbial cathodes, Electrochim. Acta 56 (2011) 2682-2688.

[49] Z. Jiang, X. Dai, H. Middleton. Investigation on passivity of titanium under steady-state conditions in acidic solutions, Mater. Chem. Phys. 126 (2011) 859-865.

[50] D. D. Macdonald. Passivity - the key to our metals-based civilization, Pure Appl. Chem. 71 (1999) 951-978.

[51] A. J. Bard and L. R. Faulkner, Electrochemical Methods: Fundamentals and Applications, John Wiley & Sons, New York, NY, 2001.

[52] J. O. Bockris, A. K. N. Reddy, and M. Gamboa-Aldeco, Modern Electrochemistry 2A: Fundamentals of Electrodics, Kluwer Academic Publishers, 2000.

[53] J. Pan, C. Leygraf, R. F. A. Jargelius-Pettersson, J. Linden. Characterization of High-Temperature Oxide Films on Stainless Steels by Electrochemical-Impedance Spectroscopy, Oxid. Met. 50 (1998) 431-455.

[54] E. Sikora, J. Sikora, D. D. Macdonald. A new method for estimating the diffusivities of vacancies in passive films, Electrochim. Acta 41 (1996) 783-789.

[55] Y. F. Cheng, C. Yang, J. L. Luo. Determination of the diffusivity of point defects in passive films on carbon steel, Thin Solid Films 416 (2002) 169-173.

[56] C. Y. Chao, L. F. Lin, D. D. Macdonald. A Point Defect Model for Anodic Passive Films, J. Electrochem. Soc. 128 (1981) 1187-1194.

[57] M. Bojinov. The ability of a surface charge approach to describe barrier film growth on tungsten in acidic solutions, Electrochim. Acta 42 (1997) 3489-3498.

[58] X. Guo, H. Imaizumi, K. Katoh. The behavior of passive films on carbon steel in sulfuric acid solutions, J. Electroanal. Chem. 383 (1995) 99-104.

[59] M. Gojic, D. Marijan, L. Kosec. Electrochemical Behavior of Duplex Stainless Steel in Borate Buffer Solution, CORROSION 56 (2000) 839-848.

[60] D. D. Macdonald, M. Urquidi-Macdonald. Theory of Steady-State Passive Films, J. Electrochem. Soc. 137 (1990) 2395-2402.

Tables captions

Table 1. Composition of both non-polluted and polluted seawater samples, given by the Spanish Institute of Geodesy.

Table 2. Electrochemical parameters for AISI 316L SS in both non-polluted and polluted seawater, obtained from cyclic polarization curves.

Table 3. Equivalent circuit parameters obtained by fitting the experimental results of EIS, for AISI 316L SS in both non-polluted and polluted seawater, at the different film formation potentials within the passive range.

Table 4. Acceptor and donor densities (N_A and N_D, respectively) for AISI 316L SS in both non-polluted and polluted seawater, at the different film formation potentials within the passive range.

Table 5. Thicknesses of the inner (W_i) and outer (W_o) space charge layers for AISI 316L SS in both non-polluted and polluted seawater, at the different film formation potentials within the passive range.

Figures captions

Fig. 1. Map showing the zones near the island of El Hierro where the non-polluted and polluted seawater samples were taken.

Fig. 2. Potentiodynamic polarization cyclic curves for AISI 316L SS in both non-polluted and polluted seawater solutions at 25º C.

Fig. 3. Current density transients for AISI 316L SS recorded after stepping the potential from the cathodic cleaning value (-0.4 $V_{Ag/AgCl}$) to the film formation potential (-0.1 $V_{Ag/AgCl}$), in both non-polluted and polluted seawater at 25º C.

Fig. 4. Nyquist (a) and Bode (b) plots for AISI 316L SS in both non-polluted and polluted seawater at 25º C, at a film formation potential of -0.1 $V_{Ag/AgCl}$.

Fig. 5. Kramers–Kronig transforms of EIS data for AISI 316L SS in (a) non-polluted seawater and (b) polluted seawater.

Fig. 6. Representation of the equivalent circuit proposed for the interpretation of EIS spectra of AISI 316L SS in the seawater solutions under study, at a film formation potential of -0.1 $V_{Ag/AgCl}$.

Fig. 7. Capacitance-potential curve obtained at 5 kHz for AISI 316L SS in the non-polluted seawater at 25º C, scanning the potential from the film formation value of 0 $V_{Ag/AgCl}$ in the negative direction.

Fig. 8. Capacitance-potential curves obtained at different frequencies for AISI 316L SS in the non-polluted seawater at 25º C, scanning the potential from the film formation value of 0 $V_{Ag/AgCl}$ in the negative direction.

Fig. 9. Mott-Schottky plots for AISI 316L SS obtained at 5 kHz at different film formation potentials in (a) non-polluted seawater, and (b) polluted seawater, at 25º C.

Fig. 10. Schematic representation of the electronic energy band for the passive film formed on AISI 316L SS surface in both non-polluted and polluted seawater, at potentials higher and lower than the flat-band potential, E_{FB}.

Fig. 11. Estimated values of the steady-state thickness of the passive film formed on AISI 316L SS surface (L_{SS}) as a function of the film formation potential, in both non-polluted and polluted seawater at 25º C.

Fig. 12. Donor density (N_D) as a function of the film formation potential for AISI 316L SS in both non-polluted and polluted seawater at 25º C.

Value	Unpolluted seawater	Polluted seawater
pH	8.02	6.23
Conductivity (μS cm^{-1})	65850	66400
Sodium (mg l^{-1})	11080	11868
Potassium (mg l^{-1})	438	447
Calcium (mg l^{-1})	558	400
Magnesium (mg l^{-1})	1486	1320
Sulphates (mg l^{-1})	2400	2600
Chlorides (mg l^{-1})	20926	21200
Bicarbonates (mg l^{-1})	159	220
Carbonates (mg l^{-1})	5.53	0.00

LiBr Solution	E_{corr} vs (Ag/AgCl)/mV	i_{corr}/μA cm^{-2}	i_p/μA cm^{-2}	E_p vs (Ag/AgCl)/mV	E_{rp} vs (Ag/AgCl)/mV	i_{rp}/mA cm^{-2}	E_p - E_{rp}/mV
0.2 M	-124 ± 7	0.30 ± 0.09	2.32 ± 0.15	557 ± 10	164 ± 10	10.95 ± 3.27	40 ± 5
0.6 M	-147 ± 10	0.58 ± 0.10	3.08 ± 0.22	496 ± 8	145 ± 12	11.89 ± 1.14	64 ± 12

	E vs (Ag/AgCl)/mV	R_S/Ω cm^2	R_1/kΩ cm^2	C_1/μF cm^{-2}	α_1	σ/kΩ cm^2 s$^{-1/2}$
Non-polluted seawater	-100	4.75 ± 0.3	385.17 ± 71	44.13 ± 0.3	0.90 ± 0.01	34.04 ± 11
	-50	5.19 ± 0.5	363.89 ± 65	39.48 ± 2	0.91 ± 0.01	41.67 ± 9
	0	5.44 ± 0.6	724.56 ± 123	39.87 ± 1	0.91 ± 0.02	45.46 ± 5
	50	5.30 ± 0.5	620.49 ± 82	33.65 ± 1	0.92 ± 0.01	52.52 ± 12
	100	5.29 ± 0.7	522.37 ± 67	26.01 ± 3	0.86 ± 0.01	67.96 ± 4
	150	5.39 ± 0.2	1143.30 ± 154	29.12 ± 4	0.88 ± 0.01	94.25 ± 17
Polluted seawater	-100	5.34 ± 0.1	249.67 ± 14	56.42 ± 5	0.92 ± 0.01	31.90 ± 7
	-50	5.13 ± 0.3	257.69 ± 9	52.21 ± 0.3	0.92 ± 0.01	34.23 ± 4
	0	5.01 ± 0.2	300.39 ± 42	43.22 ± 2	0.92 ± 0.01	36.67 ± 9
	50	5.20 ± 0.1	372.93 ± 83	37.21 ± 2	0.92 ± 0.01	42.48 ± 1
	100	5.43 ± 0.2	393.69 ± 24	30.34 ± 3	0.92 ± 0.01	53.33 ± 1
	150	5.64 ± 0.4	734.25 ± 54	27.42 ± 4	0.91 ± 0.01	55.63 ± 3

	Non-polluted seawater		Polluted seawater	
***E* vs (Ag/AgCl)/V**	N_A **/ 10^{20}cm^{-3}**	N_D **/ 10^{20}cm^{-3}**	N_A **/ 10^{20}cm^{-3}**	N_D **/ 10^{20}cm^{-3}**
-0.10	7.83 ± 0.2	3.52 ± 0.07	7.43 ± 0.2	10.10 ± 1
-0.05	6.71 ± 0.3	3.04 ± 0.01	9.05 ± 0.1	9.06 ± 1
0	4.81 ± 0.03	1.75 ± 0.3	6.07 ± 0.5	6.84 ± 2
0.05	3.63 ± 0.5	1.39 ± 0.2	5.70 ± 0.6	4.93 ± 0.2
0.10	1.70 ± 0.01	1.23 ± 0.06	5.51 ± 0.5	3.84 ± 0.1
0.15	1.22 ± 0.2	0.96 ± 0.09	6.92 ± 0.6	3.47 ± 0.4

	Non-polluted seawater		Polluted seawater	
***E* vs (Ag/AgCl)/mV**	W_i / nm	W_o / nm	W_i / nm	W_o / nm
-0.10	0.64 ± 0.02	0.89 ± 0.01	0.85 ± 0.02	0.56 ± 0.04
-0.05	0.58 ± 0.02	0.94 ± 0.02	0.87 ± 0.04	0.63 ± 0.04
0	0.71 ± 0.03	1.18 ± 0.07	0.89 ± 0.05	0.72 ± 0.05
0.05	0.75 ± 0.02	1.43 ± 0.04	0.83 ± 0.01	0.80 ± 0.02
0.10	0.87 ± 0.05	1.50 ± 0.06	0.87 ± 0.05	0.84 ± 0.01
0.15	1.23 ± 0.05	1.97 ± 0.05	1.06 ± 0.11	1.06 ± 0.12

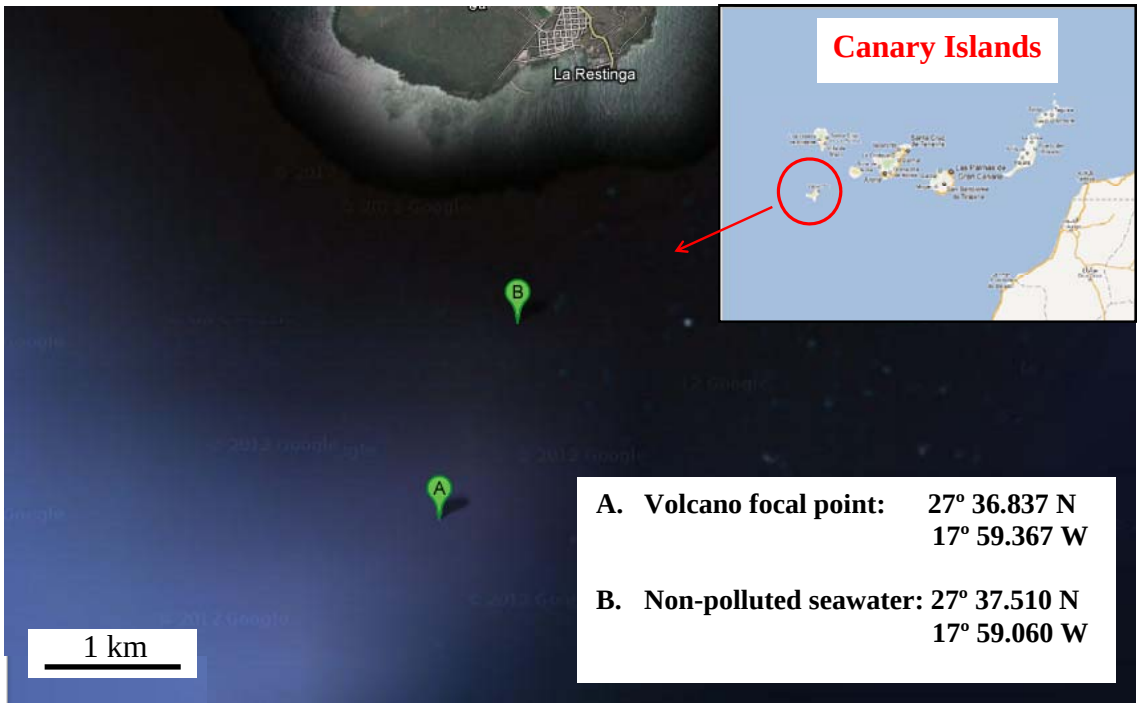
Canary Islands
La Restinga
B
A
1 km
A. Volcano focal point: 27º 36.837 N
17º 59.367 W
B. Non-polluted seawater: 27º 37.510 N
17º 59.060 W

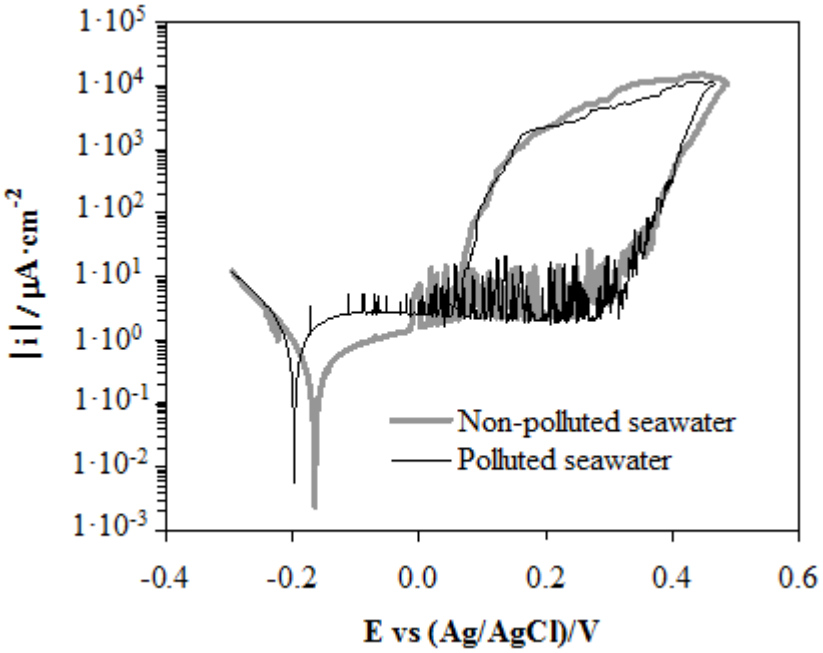
1·10^5
1·10^4
1·10^3
1·10^2
1·10^1
1·10^0
1·10^-1
1·10^-2
1·10^-3
|i| / μA·cm^-2
-0.4
-0.2
0.0
0.2
0.4
0.6
E vs (Ag/AgCl)/V
Non-polluted seawater
Polluted seawater

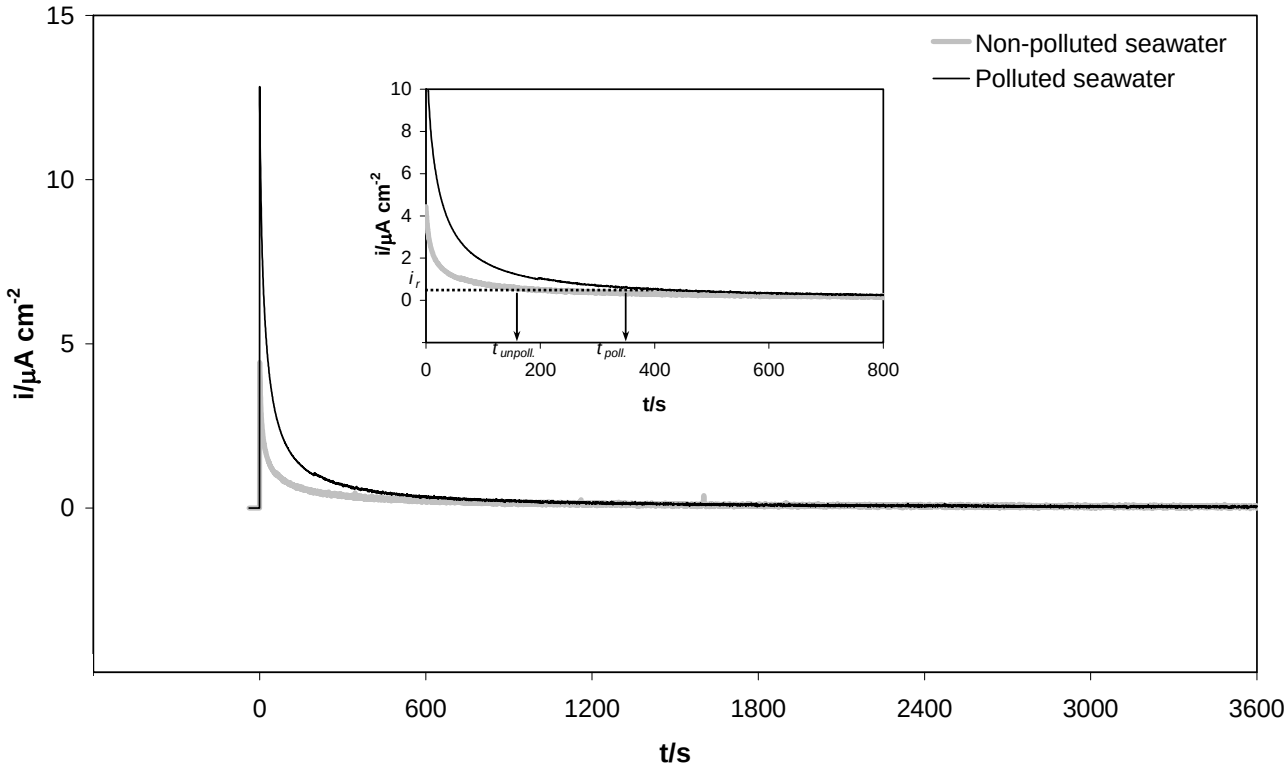
Non-polluted seawater
Polluted seawater
i/µA cm-2
t/s
15
10
5
0
0
600
1200
1800
2400
3000
3600
10
8
6
4
2
0
i/µA cm-2
ir
t unpoll.
t poll.
0
200
400
600
800
t/s

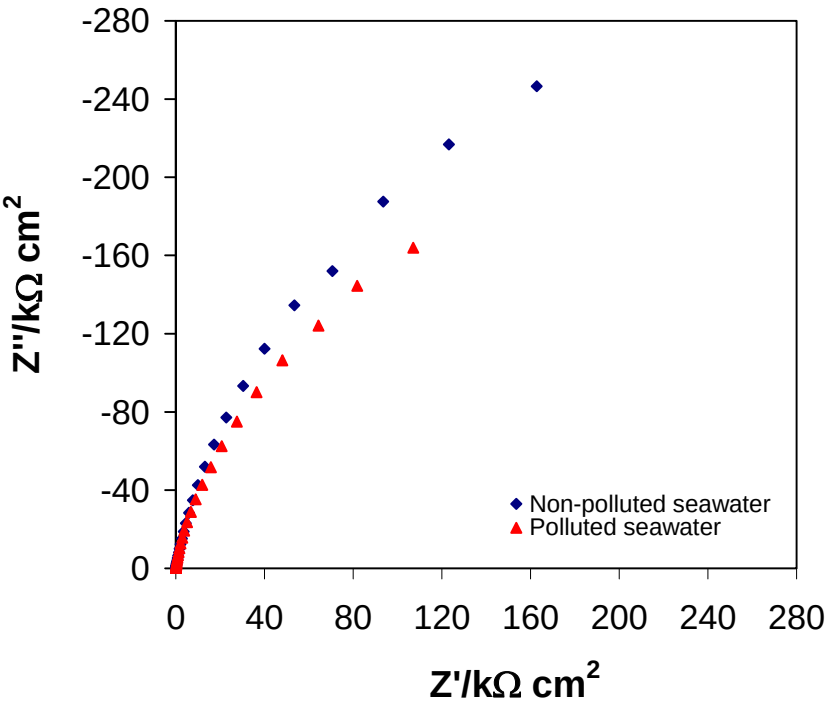
-280
-240
-200
-160
-120
-80
-40
0
Z''/kΩ cm2
0
40
80
120
160
200
240
280
Z'/kΩ cm2
Non-polluted seawater
Polluted seawater

(a)

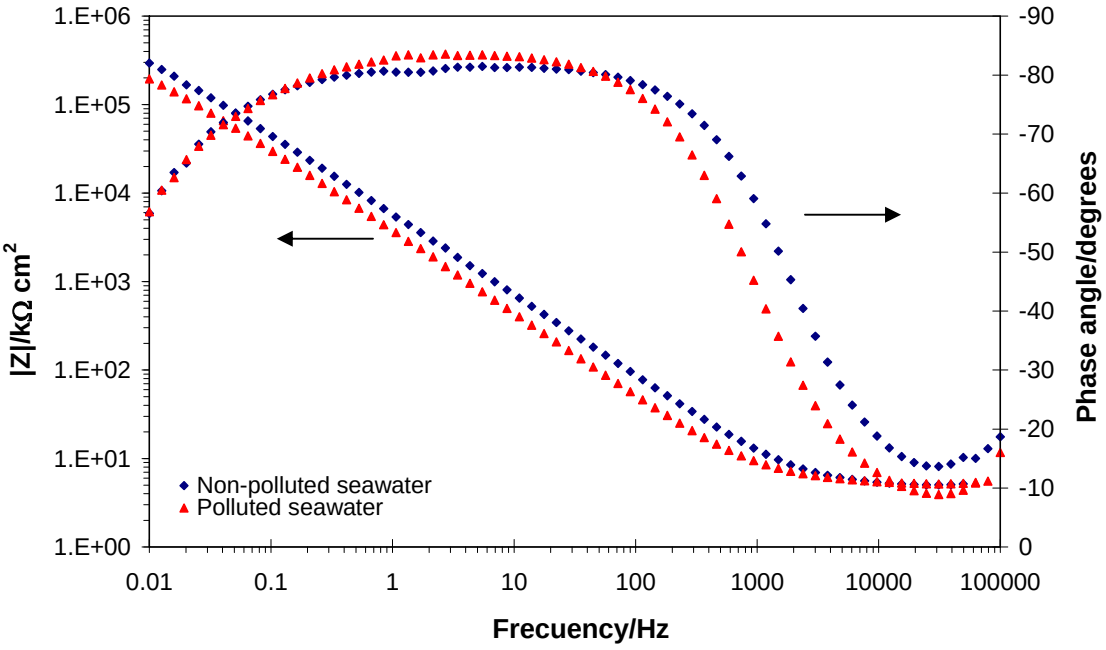
1.E+06
1.E+05
1.E+04
1.E+03
1.E+02
1.E+01
1.E+00
|Z|/kΩ cm2
-90
-80
-70
-60
-50
-40
-30
-20
-10
0
Phase angle/degrees
0.01
0.1
1
10
100
1000
10000
100000
Frecuency/Hz
Non-polluted seawater
Polluted seawater

(b)

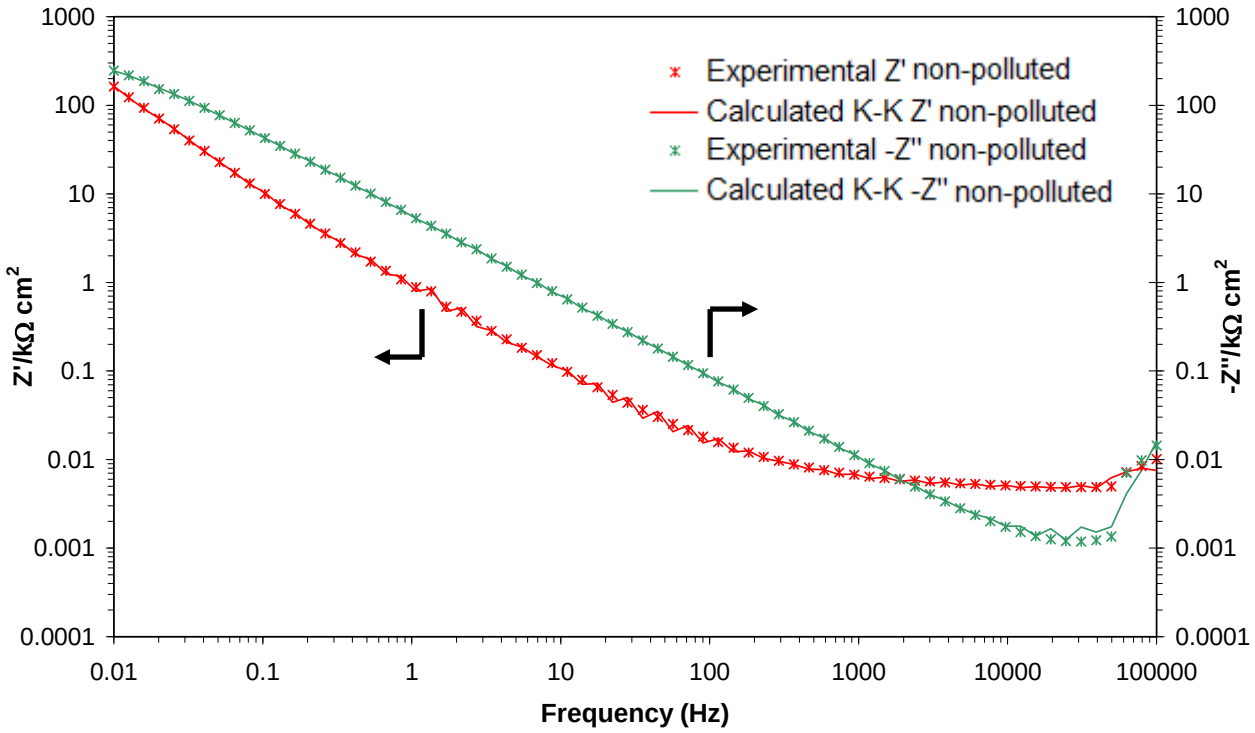
Experimental Z' non-polluted
Calculated K-K Z' non-polluted
Experimental -Z'' non-polluted
Calculated K-K -Z'' non-polluted
Z'/kΩ cm²
-Z''/kΩ cm²
Frequency (Hz)
1000
100
10
1
0.1
0.01
0.001
0.0001
0.01
0.1
1
10
100
1000
10000
100000

(a)

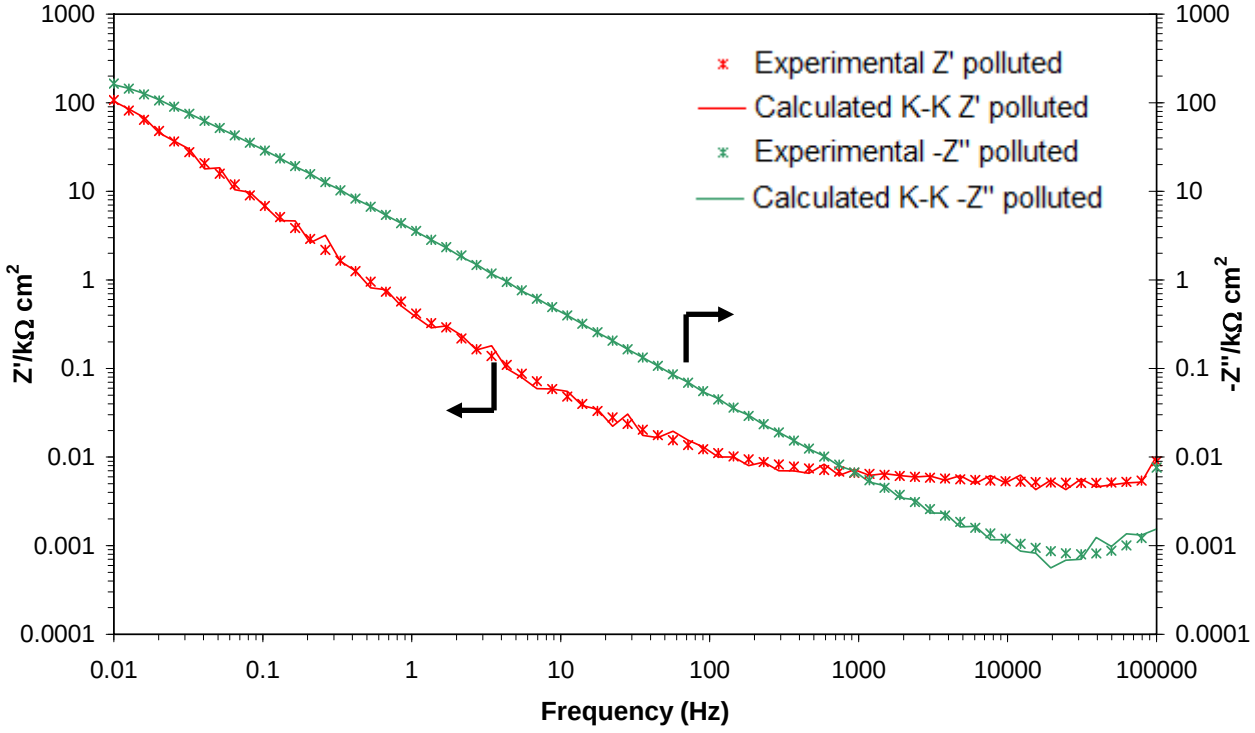
Experimental Z' polluted
Calculated K-K Z' polluted
Experimental -Z'' polluted
Calculated K-K -Z'' polluted
Z'/kΩ cm²
-Z''/kΩ cm²
Frequency (Hz)
1000
100
10
1
0.1
0.01
0.001
0.0001
0.01
0.1
1
10
100
1000
10000
100000

(b)

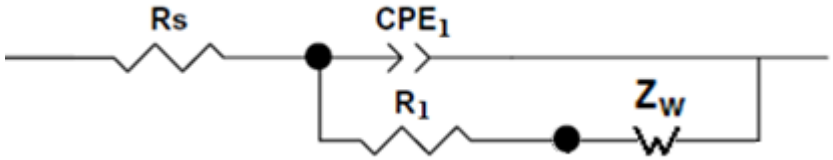
Rs
CPE1
R1
ZW

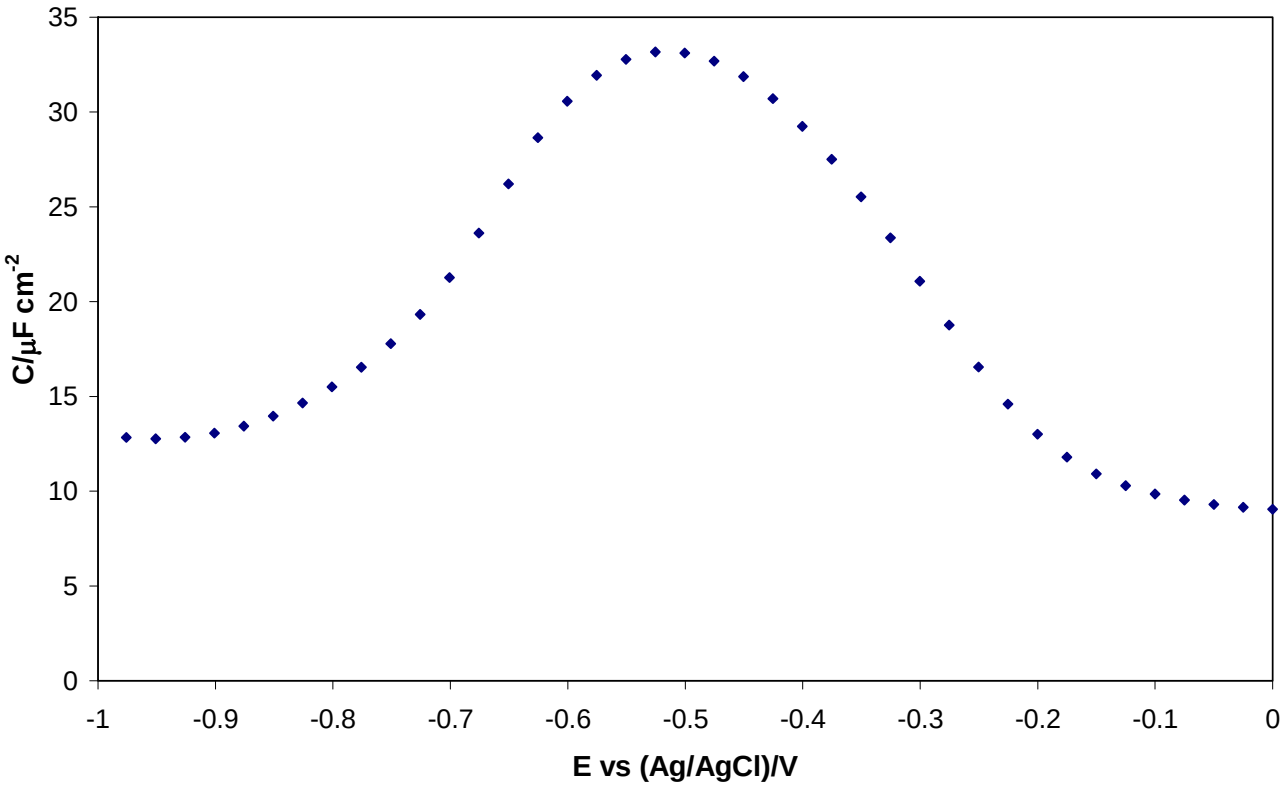
35
30
25
20
15
10
5
0
C/μF cm-2
-1
-0.9
-0.8
-0.7
-0.6
-0.5
-0.4
-0.3
-0.2
-0.1
0
E vs (Ag/AgCl)/V

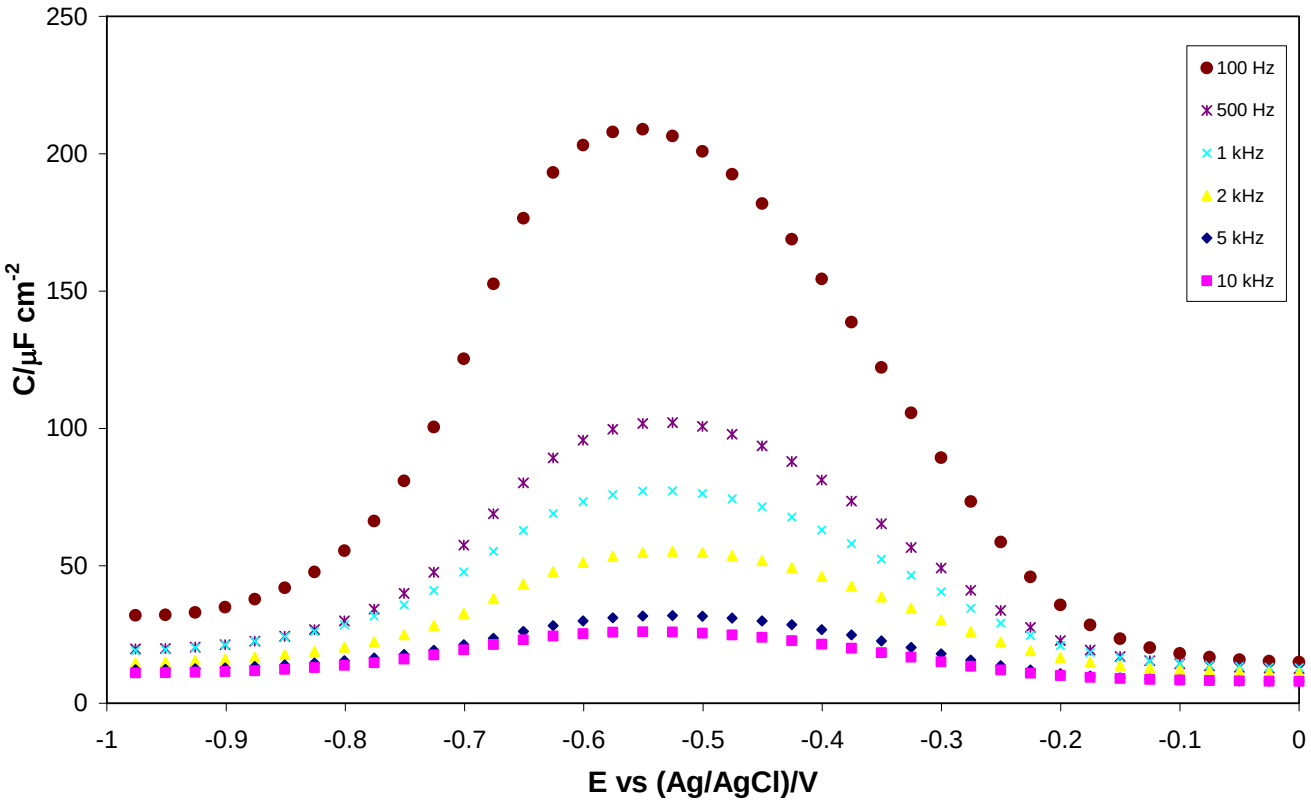
250
200
150
100
50
0
C/μF cm-2
-1
-0.9
-0.8
-0.7
-0.6
-0.5
-0.4
-0.3
-0.2
-0.1
0
E vs (Ag/AgCl)/V
100 Hz
500 Hz
1 kHz
2 kHz
5 kHz
10 kHz

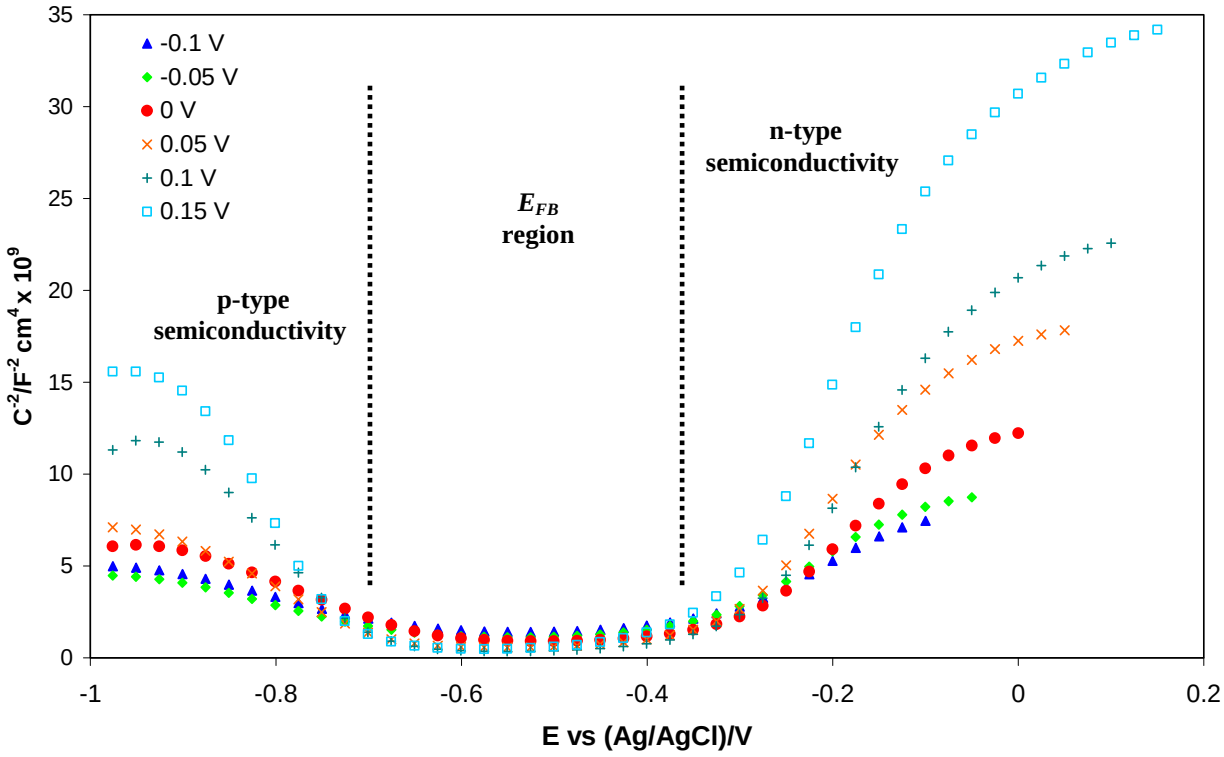
-0.1 V
-0.05 V
0 V
0.05 V
0.1 V
0.15 V
p-type semiconductivity
E_{FB} region
n-type semiconductivity
$C^{-2}/F^{-2}\,cm^4 \times 10^9$
E vs (Ag/AgCl)/V

(a)

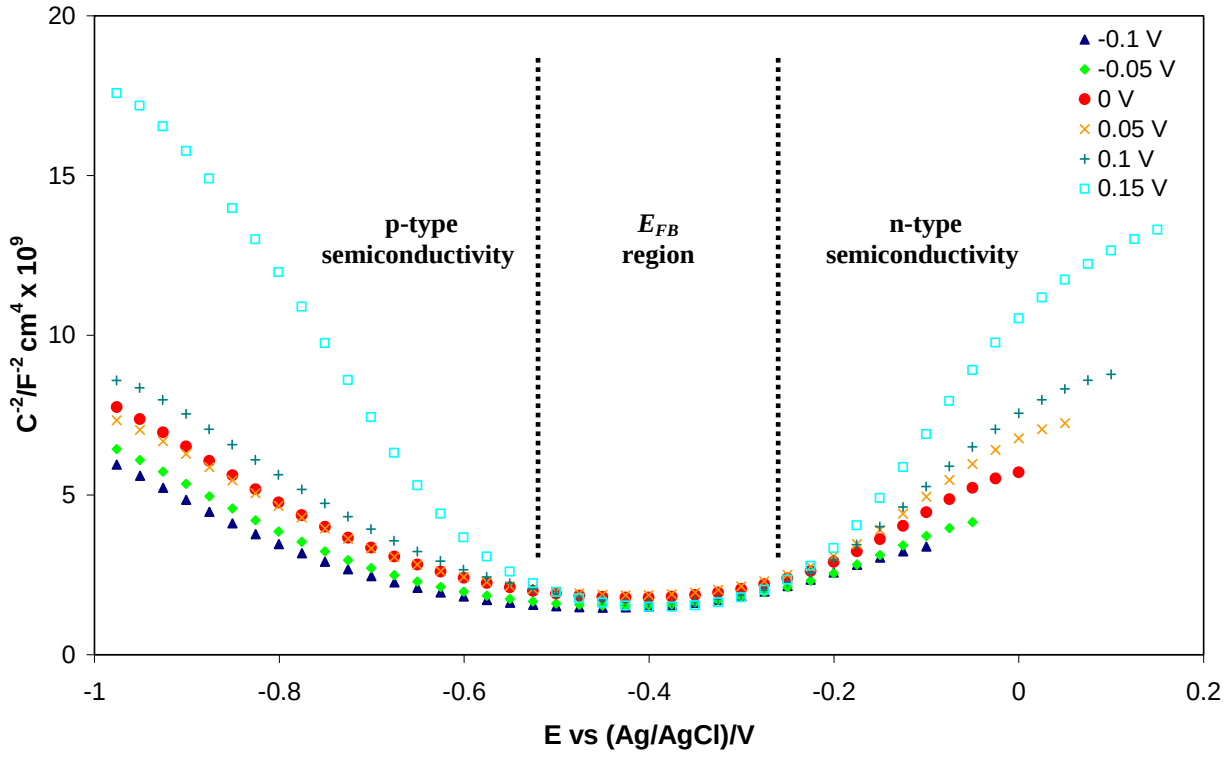
-0.1 V
-0.05 V
0 V
0.05 V
0.1 V
0.15 V
p-type semiconductivity
E_{FB} region
n-type semiconductivity
$C^{-2}/F^{-2}\,cm^4 \times 10^9$
E vs (Ag/AgCl)/V

(b)

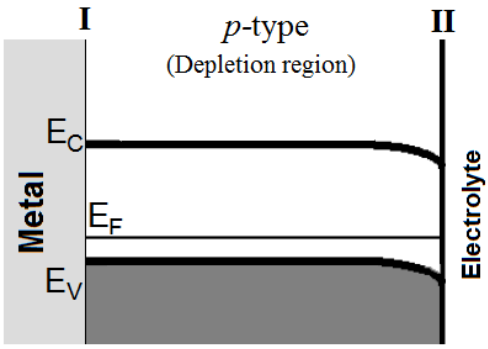
I
p-type
(Depletion region)
II
Metal
E_C
E_F
E_V
Electrolyte

$E < E_{FB}$

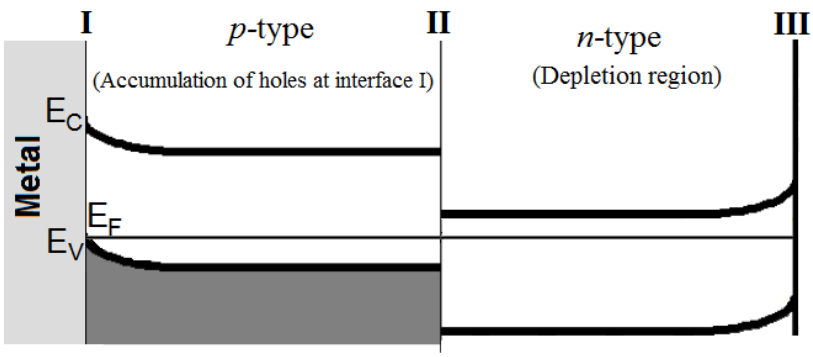
I
p-type
II
n-type
III
(Accumulation of holes at interface I)
(Depletion region)
Metal
E_C
E_F
E_V

$E > E_{FB}$

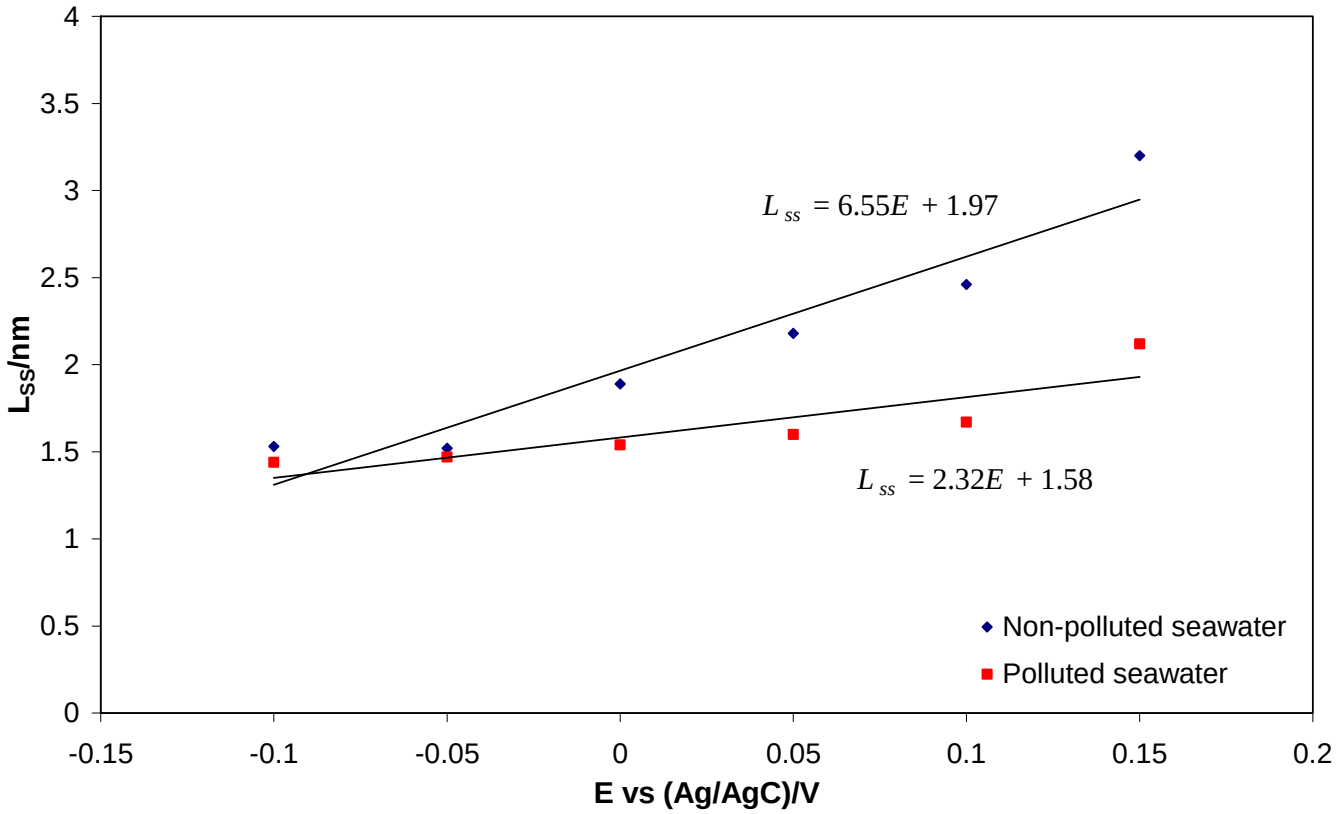
4
3.5
3
2.5
2
1.5
1
0.5
0
-0.15
-0.1
-0.05
0
0.05
0.1
0.15
0.2
Lss/nm
E vs (Ag/AgC)/V
$L_{ss} = 6.55E + 1.97$
$L_{ss} = 2.32E + 1.58$
Non-polluted seawater
Polluted seawater

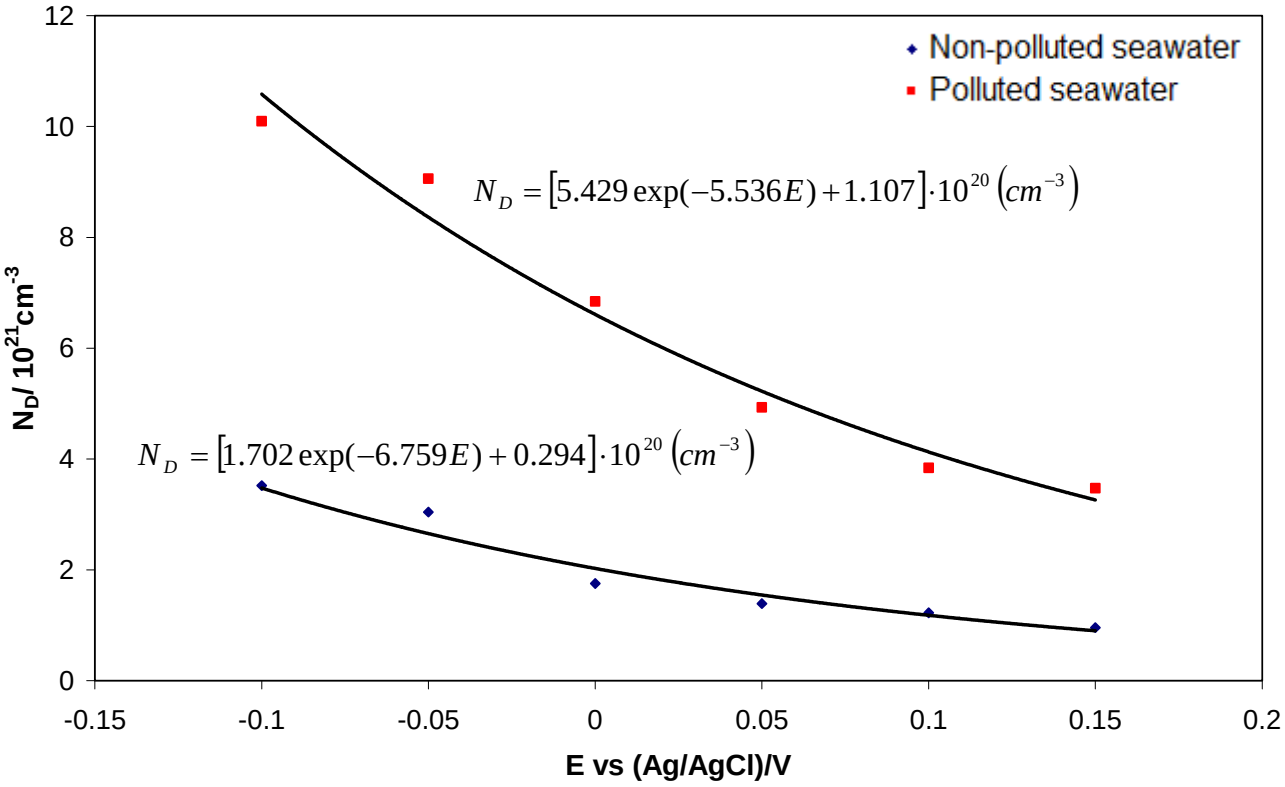
Non-polluted seawater
Polluted seawater
$N_D = [5.429\exp(-5.536E) + 1.107]\cdot 10^{20}\ (cm^{-3})$
$N_D = [1.702\exp(-6.759E) + 0.294]\cdot 10^{20}\ (cm^{-3})$
N_D/ 10^{21}cm^{-3}
E vs (Ag/AgCl)/V
12
10
8
6
4
2
0
-0.15
-0.1
-0.05
0
0.05
0.1
0.15
0.2